Small

NANO · MICRO small
www.small-journal.com

RESEARCH ARTICLE

Rational Rigid-Core Design Realizes Efficient and Color-Pure Sky-Blue MR-TADF Emission in Boron-Nitrogen Functionalized Dibenzo-Xanthene

Thamodharan Viswanathan[1] | Sabyasachi Maity[1] | Upasana Deori[1] | Nikhitha R.[2] | Nandish SH[1] | Sandhayarani Pal[1] | Nisha Yadav[1] | Anirban Mondal[2] | Pachaiyappan Rajamalli[1]

[1]Materials Research Centre, Indian Institute of Science, Bengaluru, Karnataka, India | [2]Department of Chemistry, Indian Institute of Technology Gandhinagar, Gandhinagar, Gujarat, India

Correspondence: Anirban Mondal (amondal@iitgn.ac.in) | Pachaiyappan Rajamalli (rajamalli@iisc.ac.in)

Received: 14 January 2026 | **Revised:** 23 April 2026 | **Accepted:** 25 April 2026

Keywords: high-efficiency OLEDs | multi-resonant TADF (MR-TADF) | narrowband sky-blue emission | rigid orthogonal acceptor strategy | small ΔE_{ST}

ABSTRACT

In this work, we report the strategic incorporation of a rigid 14H-dibenzo[a,j]xanthene (**DBX**) core into the **BCz-BN** framework, leading to the development of a novel **DBX-BCz-BN** multi-resonance (MR) thermally activated delayed fluorescence (TADF) emitter. This structural modification preserves the sky-blue emission color while substantially narrowing the emission profile, reducing the full width at half maximum (FWHM) to 17 nm. In addition, the singlet–triplet energy gap (ΔE_{ST}) is lowered from 0.17 eV for **BCz-BN** to 0.06 eV, thereby promoting more efficient reverse intersystem crossing (RISC) and improved exciton harvesting. As a result, the corresponding OLED device based on **DBX-BCz-BN** exhibits an external quantum efficiency (EQE) of 22.2%, while maintaining the same emission color. These results demonstrate that rigid-core engineering via DBX incorporation is an effective strategy for achieving narrowband, efficient, and color-pure sky-blue TADF emitters.

1 | Introduction

In high-resolution displays and new augmented/virtual reality (AR/VR) applications, where stringent spectral stability, low power consumption, and extended operational lifetimes are crucial, high-efficiency, high-color-purity blue emitters are among the most important parts of next-generation organic light-emitting diodes (OLEDs) [1–3]. Because organic emitters can achieve high internal quantum efficiencies without relying on rare or hazardous metals like iridium or platinum, they have gained popularity as sustainable alternatives to heavy-metal phosphors [4–9]. This is especially true of multi-resonance (MR) thermally activated delayed fluorescence (TADF) materials. MR-TADF emitters, as opposed to metal complexes, provide narrowband emission, tunable molecular design, and superior compatibility with flexible and solution-processable device architectures [10–12]. Although considerable progress has been made, several challenges remain to be addressed. For instance, achieving ultra-narrow emission while maintaining a small singlet-triplet energy gap (ΔE_{ST}) for efficient reverse intersystem crossing (RISC) remains difficult [2, 13]. Many reported blue MR-TADF systems exhibit broadened spectra, poor color stability under operational conditions, or significant efficiency roll-off at practical brightness levels [14]. Furthermore, attaining both narrow emission and photochemical stability in sky-blue materials continues to be a major challenge.

Several studies on the **BCz-BN** MR-core have shown that extending conjugation through para-substitution at the boron-linked phenyl ring is an effective strategy for tuning MR-TADF photophysics and broadening optoelectronic applications [15–18]. Representative examples include electron-deficient

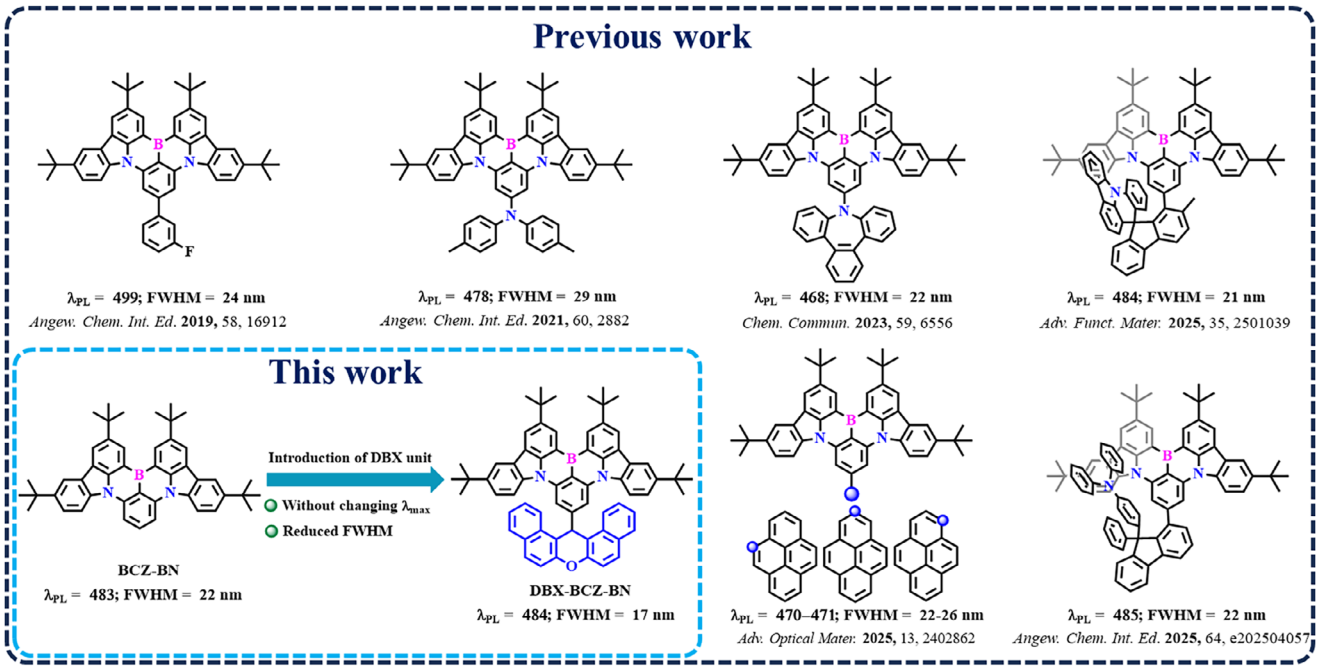

FIGURE 1 | Molecular design strategy and overview of multi-resonance molecular architectures.

derivatives that afford red-shifted yet narrowband emission, and carbazole-based DABNA analogues that enable color tuning from deep-blue to green [19, 20]. Other studies have employed donor-modified pure-blue emitters and pyrene-functionalized systems to improve device stability in hyper fluorescence OLEDs [21, 22]. More recently, compact donor–acceptor emitters have been developed to strengthen charge-transfer control while retaining narrow emission [23]. Centre-chiral frustrated Lewis pair designs have also emerged as an effective strategy to combine circularly polarized emission with high device efficiency (Figure 1) [24]. However, these advances often rely on broader emission profiles, extensive device-level optimization, and increased molecular complexity, including the incorporation of double/multiple boron atoms within the MR framework or elaborate peripheral substituents used to control molecular orientation and device performance [23, 25, 26]. While effective, such strategies can compromise synthetic accessibility and scalability.

To address these challenges, we introduce a rational design strategy based on the para-linked incorporation of a rigid dibenzo[xanthene] (**DBX**) unit into the **BCz-BN** MR core through a non-conjugated architecture. This approach preserves the intrinsic multi-resonance electronic structure while increasing molecular rigidity and steric protection. The highly twisted configuration (~87°) effectively suppresses π-conjugation, thereby maintaining narrowband emission, while the bulky DBX fragment modulates vibrational degrees of freedom and excited-state relaxation dynamics without significantly perturbing the frontier orbitals. In addition, the modular synthetic strategy enables straightforward functionalization and scalability. Collectively, **DBX-BCz-BN** achieves a balanced combination of ultranarrow emission, reduced ΔE_{ST} and efficient RISC through a relatively simple rigid-core modification. Accordingly, the **DBX** design strategy provides a practical and effective approach to simultaneously enhance color purity while preserving emission wavelength and device performance, without introducing significant synthetic complexity, thereby offering an attractive alternative to strategies that focus solely on maximizing EQE.

2 | Results and Discussion

2.1 | Molecular Design, Synthesis, and Theoretical Calculations

The molecular design of **DBX-BCz-BN** incorporates a **DBX** core, connected to the **BCz-BN** multi-resonance acceptor unit at the para-position [21]. The incorporation of the **DBX** core introduces a rigid and extended polycyclic framework, enhancing structural stability while enforcing a well-defined spatial arrangement.

The target MR-TADF material, **DBX-BCz-BN**, was synthesized via a three-step procedure. In the first step, 14-(4-bromophenyl)-3,5-difluoro-14H-dibenzo[a,j]xanthene (precursor) was prepared through the cyclisation of 4-bromo-3,5-difluorobenzaldehyde with 2-naphthol [27]. The precursor was then coupled with di-tert-butyl-9H-carbazole via a nucleophilic substitution reaction to yield the intermediate DBX-BCzBr. Finally, a boron insertion reaction using BBr_3 afforded the target **DBX-BCz-BN** with yields up to 21% (Scheme S1). Detailed synthetic procedures for both the precursor and the final material are provided in the Supporting Information. Structural characterization of the compounds was performed using ^{1}H and ^{13}C NMR spectroscopy, as well as high-resolution mass spectrometry (HRMS), with full spectra shown in the (Figures S1–S8). Prior to device fabrication, **DBX-BCz-BN** was further purified by temperature-gradient high-vacuum sublimation to ensure high purity.

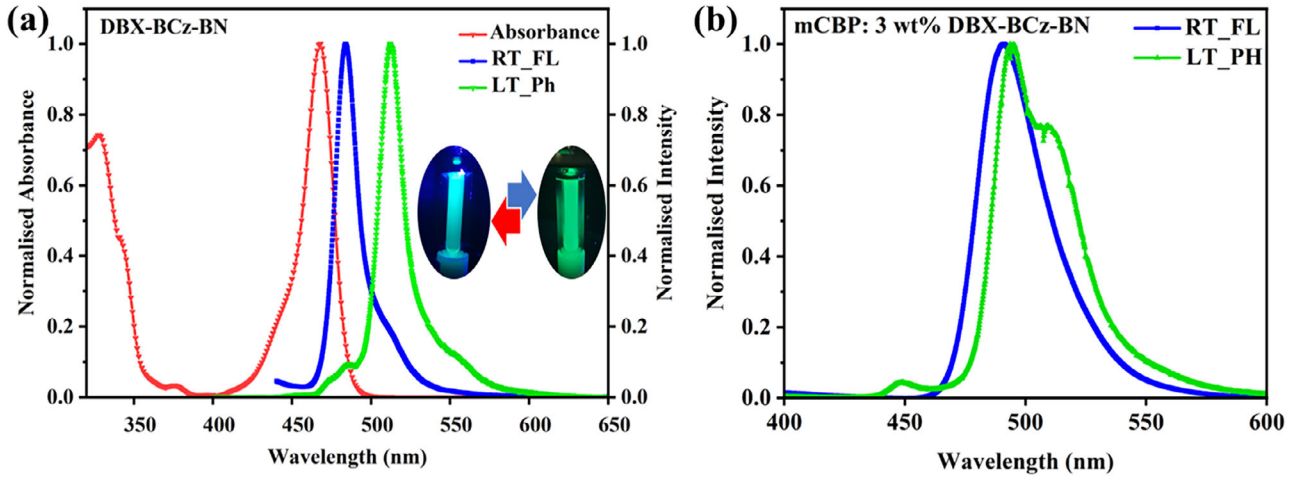

FIGURE 2 | (a) Absorbance (red) and Emission spectra (RT (blue) and 77 K (green) of **DBX-BCz-BN** in toluene solution (1×10^{-5} M); inset: photographs of the **DBX-BCz-BN** in toluene at RT and 77 K under 365 nm irradiation. (B) Emission spectra of **DBX-BCz-BN** in 3 wt.% in mCBP at RT (blue) and 77 K (green).

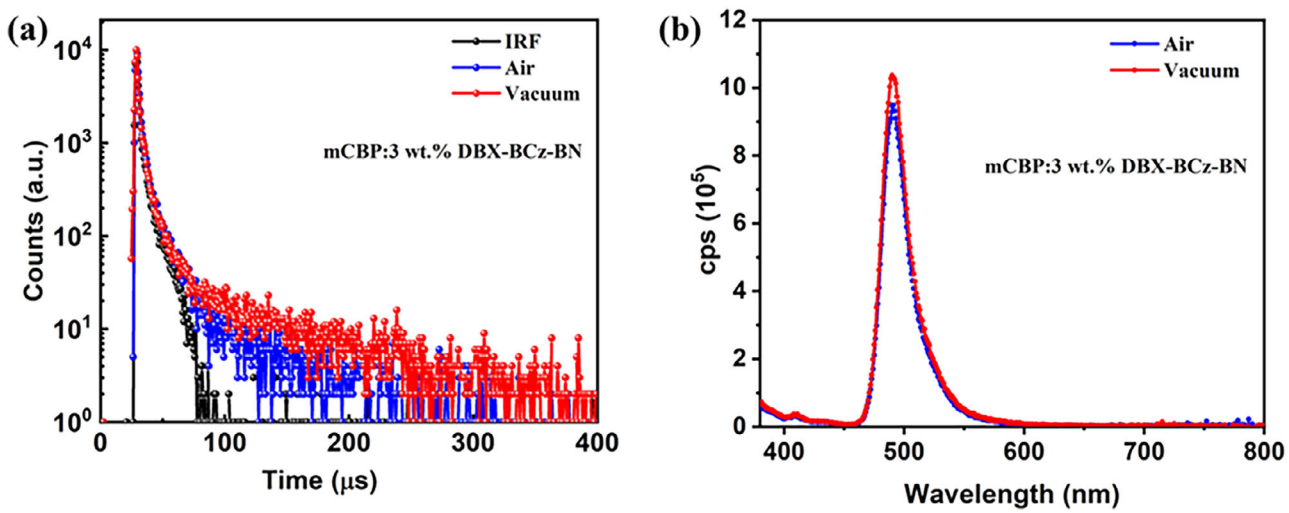

FIGURE 3 | (a) Lifetime profile of **DBX-BCz-BN** in 3 wt.% in mCBP in air (blue) and vacuum (red). (b) Emission spectra of **DBX-BCz-BN** in 3 wt.% in mCBP in air (blue) and vacuum (red).

2.2 | Photophysical Properties

The photophysical characteristics of **DBX-BCz-BN** were investigated in toluene solution and in 3 wt.% *m*CBP-doped films (Figures 2, 3 and Table 1), and the results were compared with those of the reference compounds (Figure 1). In toluene, **DBX-BCz-BN** exhibited three distinct absorption features centered at 328, 375, and 468 nm, corresponding to the π–π^* transition localized within the rigid MR skeleton and a low-energy intramolecular charge-transfer (ICT) transition from the donor (BCz) to the boron-nitrogen acceptor framework. The absorption profile of **DBX-BCz-BN** closely resembles that of **BCz-BN**, which exhibits an ICT peak at 467 nm, but the slightly red-shifted absorption tail in **DBX-BCz-BN** indicates stronger donor–acceptor electronic coupling facilitated by the extended conjugation imparted by the DBX unit.

In the photoluminescence spectra, **DBX-BCz-BN** displayed an intense sky-blue emission at 484 nm in toluene with a narrow FWHM of 17 nm (Figure 2), indicative of a highly localized short-range charge-transfer (SRCT) transition typical of MR-TADF emitters. In comparison, reported materials (Figure 1) emitted at 468–485 nm with FWHMs of 21–24 nm, respectively. The emission of **DBX-BCz-BN** is slightly red-shifted relative to both analogues, reflecting the enhanced π-extension and improved conjugation through the DBX linkage, which subtly stabilizes the LUMO and narrows the optical gap. The small Stokes shift (16 nm) observed for **DBX-BCz-BN** confirms limited geometric relaxation between the ground and excited states, consistent with the rigid MR core along with the **DBX** unit. Subsequently, the solvatochromic behavior of **DBX-BCz-BN** was evaluated in various solvent polarities, including *n*-hexane, toluene, THF, and DCM (Figure S9 and Table S1). The photoluminescence spectra exhibited a subtle positive solvatochromic shift in emission

TABLE 1 | Photophysical data of **DBX-BCz-BN** in toluene solution (1×10^{-5} M) and doped film (mCBP).

Emitter	In toluene solution (1×10^{-5} M)[a]										
	λ_{abs} (nm)	$\lambda_{em}{}^{max}$ (nm)	FWHM (nm)	S_1 (eV)	T_1 (eV)	ΔE_{ST} (eV)	Φ %	τ (µs)	k_F [10^7 s^{-1}]		
DBX-BCz-BN	328, 375, 468	484	17	2.65	2.50	0.15	33	0.012	2.8		
	In 3 wt.% *m*CBP host-blended film[a]										
	$\lambda_{em}{}^{max}$ (nm)	FWHM (nm)	S_1 (eV)	T_1 (eV)	ΔE_{ST} (eV)	Φ_P %	Φ_D %	Φ_{PL} %	τ_P (µs)	τ_D (µs)	k_{ISC} [10^7 s^{-1}]	k_{RISC} [10^5 s^{-1}]
	491	30	2.64	2.58	0.06	42	54	96[b]	0.006	14.5	9.4	1.6

[a]Measured under ambient conditions.

[b]Measured under an inert atmosphere.

maxima from 477 nm in nonpolar *n*-hexane to 490 nm in polar DCM, with FWHM values remaining narrow and varying slightly from 16 nm (hexane) to 25 nm (DCM). This limited bathochromic shift and preservation of narrow emission bands are characteristic of MR-TADF emitters, where the excited state is dominated by SRCT character localized within the rigid MR framework. Unlike typical long-range CT states that display broader and more pronounced solvent-dependent shifts due to extensive dipole moment changes, the SRCT nature inherent to MR-TADF compounds leads to weak solvent stabilization effects. The modest increase in FWHM in more polar solvents likely reflects minor solvent reorganization without significant geometric relaxation of the emitter [28]. These results affirm that **DBX-BCz-BN** maintains its highly localized emissive state across different solvent environments, supporting the expected MR-TADF mechanism with sharp, well-defined emission even under varying polarity.

In the doped film (3 wt.% in *m*CBP, Figure 2b), **DBX-BCz-BN** exhibited an emission maximum at 491 nm with a marginally increased narrowband emission character. The slight red shift compared to the solution spectrum indicates weak host-guest interactions and negligible aggregation effects, demonstrating the robustness of the MR framework in the solid state [29]. The S_1 and T_1 energy levels derived from the onset of fluorescence and phosphorescence spectra were 2.64 eV and 2.58 eV, respectively, corresponding to a small ΔE_{ST} of 0.06 eV in the doped film, whereas in toluene solution, the S_1 and T_1 levels were found to be 2.65 eV and 2.50 eV, respectively, giving a ΔE_{ST} of 0.15 eV. Both these ΔE_{ST} values are smaller than those of **BCz-BN** (0.17 eV), suggesting efficient RISC due to the finely balanced orbital separation and MR-induced short-range CT character. Photoluminescence quantum yield (PLQY) measurements further support the superior emissive efficiency of **DBX-BCz-BN**, reaching 33% in toluene, 42% in the mCBP-doped film under ambient conditions, and an excellent 96% under inert atmosphere, highlighting the strong suppression of nonradiative quenching in the solid-state environment. These values surpass those of **BCz-BN** and are equal to those of **TBA-BCz-BN** (95%), yet they highlight the excellent PLQY of the **DBX**-modified structure. In doped film the prompt lifetime was determined to be 6.1 ns (Figure S10), while the average delayed lifetimes of **DBX-BCz-BN** were measured to be 14.5 µs in ambient and 20.5 µs in vacuum conditions, as shown in Figure 3a, significantly shorter than that of **BCz-BN** (60 µs), implying a faster RISC process, which is beneficial for reducing triplet accumulation and exciton quenching in device operation. Figure 3b shows the increase in photoluminescence intensity under air and vacuum conditions, suggesting the involvement of triplet excitons. The calculated radiative and nonradiative rate constants are $k_r^S = 1.6 \times 10^8$ s^{-1} and $k_{nr}^S = 6.7 \times 10^6$ s^{-1}, further confirming the highly efficient singlet emission and negligible non-radiative losses. The k_{ISC} and k_{RISC} rate constants are 9.4×10^7 s^{-1} and 1.6×10^5 s^{-1}, respectively. These results demonstrate a balanced intersystem-crossing mechanism conducive to efficient TADF behaviour.

To elucidate the structure-property relationships and rationalize the experimentally observed photophysical behavior, density functional theory (DFT) and time-dependent DFT (TD-DFT) calculations were performed. Particular attention was given to understanding how the non-conjugated, sterically twisted **DBX** unit modulates the electronic structure and excited-state characteristics of the **BCz-BN** framework while preserving its intrinsic multiresonance (MR) nature. Ground- and excited-state geometries were optimized using the B3LYP functional with the def2-TZVP basis set and D3BJ dispersion correction, as implemented in the ORCA software package (Tables S5 and S6) [30]. Accurate excited-state energies were further evaluated using TD-DFT with the double-hybrid B2PLYP functional within the Tamm–Dancoff approximation (TDA), employing the def2-TZVP basis set and D3BJ dispersion correction, with toluene included as the solvent [31]. For the unsubstituted **BCz-BN** emitter, the absence of the bulky **DBX** fragment preserves the intrinsic MR electronic structure, giving HOMO and LUMO energies of −5.95 eV and −0.84 eV, respectively (Figure 4). The calculated singlet ($S_1 = 2.65$ eV) and triplet ($T_1 = 2.52$ eV) energies yield a ΔE_{ST} of 0.13 eV, which is consistent with efficient TADF behavior. The predicted emission maximum at 468 nm with a slightly higher oscillator strength ($f = 0.47$) reflects a more allowed transition arising from minimal perturbation of the MR framework (Table S4).

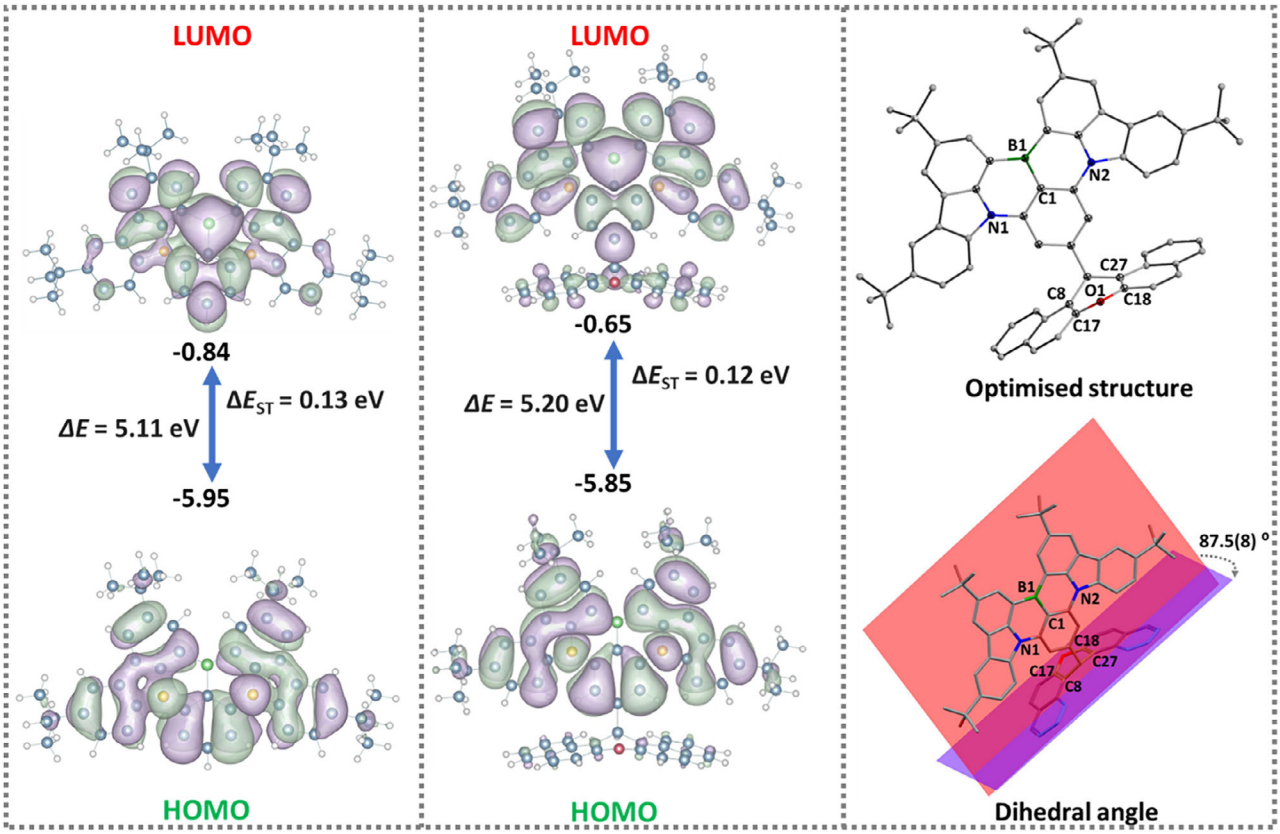

FIGURE 4 | Left: Frontier molecular orbitals (HOMO and LUMO) of the **BCz-BN** MR emitter. Middle: Frontier molecular orbitals (HOMO and LUMO) of the **DBX-BCz-BN** MR emitter. Right: Optimized molecular structure and dihedral angle of the **DBX-BCz-BN** MR emitter obtained from DFT and TD-DFT calculations. The dihedral angle is defined between the red plane formed by the B1–N1–C1–N2 atoms of the BCz-BN core and the blue plane formed by the C8–C17–C18–C27 atoms of the DBX core.

Upon incorporation of the rigid **DBX** unit, both excited-state energies are elevated to $S_1 = 2.73$ eV and $T_1 = 2.61$ eV, resulting in a comparable ΔE_{ST} of 0.12 eV, in good agreement with the experimentally determined solution-state value (Table S4 and Figure 4). A corresponding blue-shifted emission maximum at 453 nm is predicted, with a comparable oscillator strength of $f = 0.43$. Frontier molecular orbital analysis shows that the HOMO (−5.85 eV) remains predominantly localized on the electronegative nitrogen atoms of the **BCz-BN** core, whereas the LUMO (−0.65 eV) extends over both the **BCz-BN** and **DBX** fragments despite the noncoplanar geometry. This delocalization is attributed to favorable π^* orbital alignment, residual through-bond polarization, and σ–π mixing at the linkage, further supported by the inductive and resonance stabilization of the oxygen-bridged **DBX** framework. As a result, **DBX** modification induces a short-range charge-transfer-like LUMO distribution over the **BCz-BN** and **DBX** moieties while preserving the resonance-stabilized MR electronic framework.

To investigate vibronic coupling effects and to gain insights into the short-delayed lifetime and fast RISC rates, Huang-Rhys factors (S) and the corresponding reorganization energies (λ) were calculated for all vibrational modes of **DBX-BCz-BN** and **BCz-BN**. In **DBX-BCz-BN**, the most active high-frequency vibration is a **DBX**-localized C–H stretching mode at 3164 cm^{-1}, exhibiting a large Huang-Rhys factor ($S = 15.5$) and a reorganization energy of approximately 10^4 cm^{-1} (Figure S11a). Owing to their weak thermal population at room temperature, however, such high-frequency modes contribute little to spectral broadening and mainly produce weak vibronic sidebands [32]. More importantly, incorporation of the bulky **DBX** fragment introduces additional low-frequency vibrational modes (<1500 cm^{-1}), primarily out-of-plane C—H bending and framework deformation motions, that are absent in **BCz-BN**. These modes exhibit moderately large Huang-Rhys factors ($S \approx 7$–10) and reorganization energies exceeding 10^3 cm^{-1}, indicative of enhanced coupling between the excited state and low-frequency nuclear motions (Figure S11b). Despite these additional modes, the low-frequency vibrational manifold remains dominated by small S values (<1-2), limiting structural relaxation and thus preserving the narrow emission profile.

By comparison, **BCz-BN** is dominated by C—H bending modes with much smaller Huang-Rhys factors ($S \approx 0.1$) and lower reorganization energies (~10^1 cm^{-1}; Figure S11c), reflecting substantially weaker vibronic coupling. This reduced vibronic activity points to a limited capacity for vibronically assisted excited-state mixing in **BCz-BN**. Taken together, these findings suggest that the non-conjugated **DBX** unit modulates the excited-state landscape primarily through enhanced vibronic coupling, arising from the introduction of additional low-frequency vibrational modes. Such modes facilitate spin-vibronic coupling by promoting non-adiabatic mixing between singlet and triplet

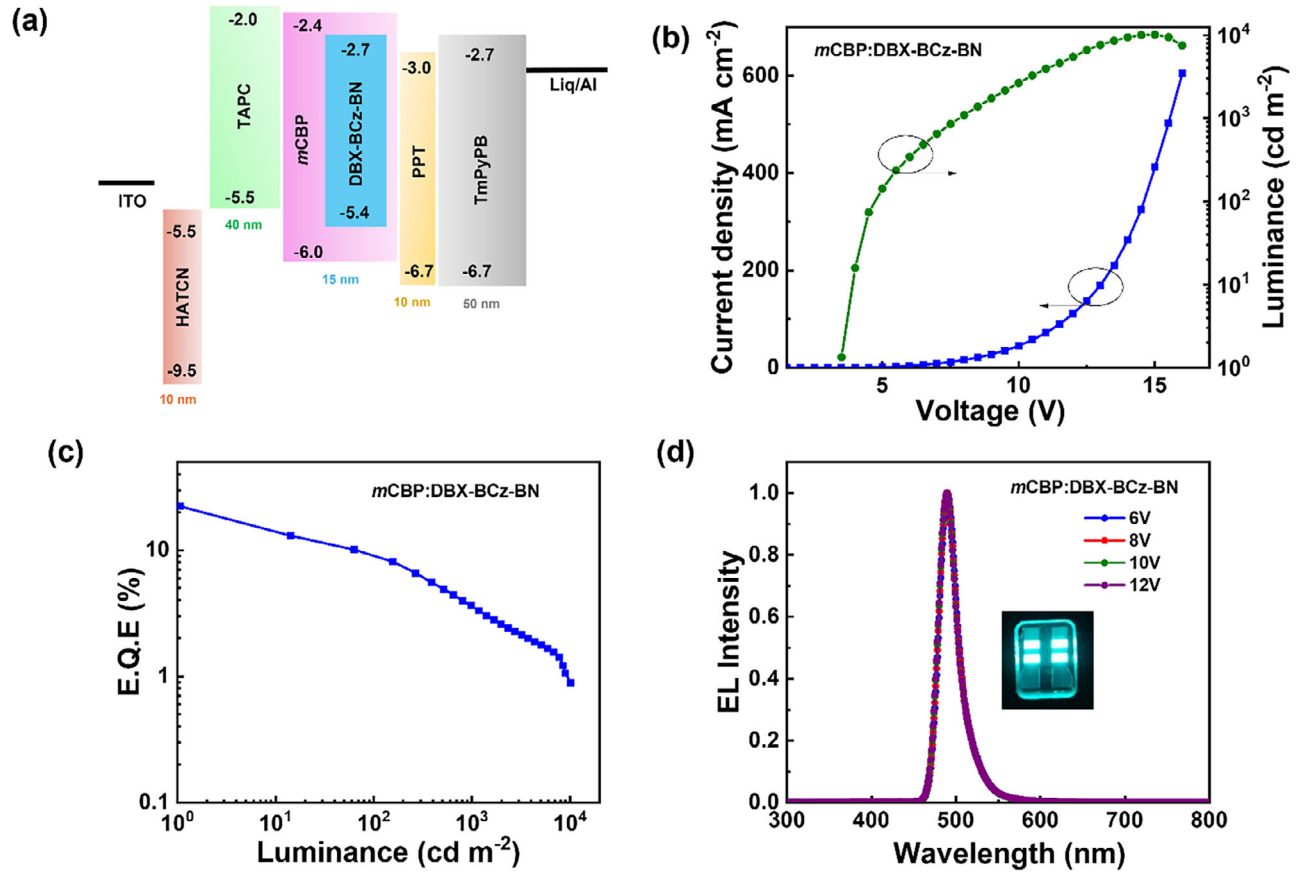

FIGURE 5 | (a) The energy level diagram of the device structure, (b) Current-Density-Voltage-Luminance (*J-V-L*) characteristics, (c) EQE vs. Luminance plots, and (d) EL spectra of the **DBX-BCz-BN** device measured at various operating voltages; inset: photograph of the device.

states, thereby accelerating RISC and contributing to the observed short delayed lifetime [33].

2.3 | Electrochemical and Thermal Properties

The electrochemical behavior of the MR-TADF emitter **DBX-BCz-BN** was studied through the cyclic voltammetric (CV) method. The measurement was conducted in dry dichloromethane containing 0.1 M of tetrabutylammonium hexafluorophosphate as the supporting electrolyte [34]. The CV curve (Figure S12) shows a quasi-reversible nature, which is typical for stable organic redox processes. The oxidation potential (E_{ox}) was observed at 1.14 V, and the reduction potential (E_{red}) was found at 1.05 V (vs. Ag/AgCl). The HOMO energy level was calculated to be −5.42 eV, and the LUMO energy level was calculated to be −2.82 eV. The calculated electrochemical band gap (ΔE) is 2.60 eV (Table S2). The relatively deep HOMO energy ensures good oxidative stability and facilitates efficient charge injection in the OLED device.

The thermal properties of **DBX-BCz-BN** were subsequently examined through thermogravimetric analysis (TGA) and differential scanning calorimetry (DSC), as shown in Figure S13. **DBX-BCz-BN** exhibits excellent thermal stability, as evidenced by a high decomposition temperature (T_d) of 511°C at 5 wt.% loss of the initial weight. Notably, this T_d value is 30°C higher than that of the parent material **BCz-BN** (481°C). This enhanced thermal robustness is attributed to the rigid and bulky nature of the DBX unit, which effectively restricts molecular motion and thermal degradation. The DSC analysis revealed a clear glass transition temperature (T_g) at 165°C. A high T_g is vital for ensuring the formation of a stable amorphous film and preventing morphological degradation during device operation. The observed high T_d and T_g values collectively indicate that **DBX-BCz-BN** possesses excellent thermal and morphological stability, making it highly favorable for the thermal vacuum evaporation process.

2.4 | Electroluminescent Properties

To explore the electroluminescence (EL) performance of the **DBX-BCz-BN** emitter, the device was fabricated with the following architecture: ITO/HATCN (10 nm)/TAPC (40 nm)/*m*CBP:3 wt.% **DBX-BCz-BN** (15 nm)/PPT (10 nm)/TmPyPB (50 nm)/Liq (2 nm)/Al (100 nm). In the structure, indium-tin-oxide (ITO) acts as a transparent anode, 1,4,5,8,9,11-Hexa azatriphenylenehexacarbonitrile (HATCN) is applied as a hole injection layer, 1,1-bis[4-[*N,N'*-di(*p*-tolyl) amino]phenyl]cyclo-hexane (TAPC) is adopted as a hole transport layer, 2,8-bis(diphenyl-phosphoryl)-dibenzo[*b,d*]thiophene (PPT) is used as an exciton blocking layer, 1,3,5-Tris(3-pyridyl-3-phenyl)benzen (TmPyPB) is utilized as an electron transport layer, 8-hydroxyquinolinolato-lithium (Liq) is used as electron injection layer and finally, aluminum

TABLE 2 | Electroluminescent properties of **DBX-BCz-BN**.

Device	V_{on} (V)	Luminance (cd m^{-2})	EQE (%)	PE (lm W^{-1})	CE (cd A^{-1})	EL (nm)	FWHM (nm)	CIE
DBX-BCz-BN	3.5	10104	22.2	33.6	37.4	488	24	(0.08, 0.38)
BCz-BN	3.5	8597	19.8	27.2	38.9	489	30	(0.09, 0.43)

(Al) serves as the cathode. A wide triplet energy gap host, 3,3'-bis(N-carbazolyl)-1,1'-biphenyl (*m*CBP), was selected to avoid back energy transfer and has well-aligned HOMO/LUMO energy levels with the adjacent layers. The device structure and energy level diagram of the materials are shown in Figure 5a. The electroluminescent properties of the **DBX-BCz-BN** OLED were recorded, including the current density-voltage-luminance (*J-V-L*) curve, EQE vs. luminance plot, and electroluminescent (EL) spectra of the OLEDs are shown in Figure 5b–d, and the detailed parameters are illustrated in Table 2.

As depicted, the device displays excellent electroluminance performance, which indicates proper exciton injection and charge transport in the device and achieves a favorable turn-on voltage of 3.5 V. The maximum EQE of 22.2% and maximum luminance of 10104 cd m^{-2} were achieved. The corresponding maximum current efficiency (CE) and power efficiency (PE) for the device are 37.4 cd A^{-1} and 33.6 lm W^{-1}, respectively (Figure S13). The device emits sky-blue emission with an EL peak maximum at 488 nm, a narrow FWHM of 24 nm, and CIE coordinates of (0.08, 0.38). Furthermore, the EL spectra at various operating voltages were measured, and no wavelength shift or emissions from the interlayers were observed, indicating effective exciton recombination and stability of the EL spectra at high voltages [35]. When compared with the reported MR-TADF emitter, the **BCz-BN**-based OLED exhibits an EQE of 19.8% and a PE of 27.2 lm W^{-1}, respectively (Figures S14 and S15, Table 2 and Table S3). The **BCz-BN** OLED shows a narrow emission FWHM of 30 nm, whereas the **DBX-BCz-BN** device exhibits an even sharper FWHM of 24 nm. The enhanced spectral purity originates from the incorporation of the rigid DBX core at the para-position of **BCz-BN**, which not only minimizes the FWHM and improves thermal stability but also preserves the emission color.

3 | Conclusions

In conclusion, we report **DBX-BCz-BN**, a novel MR-TADF emitter based on rigid-core integration of the **DBX** unit into the **BCz-BN** scaffold. This design enables simultaneous enhancement of color purity and excited-state dynamics, without compromising the emission wavelength and device performance. The **DBX** modification delivers an ultranarrow emission in solution (17 nm FWHM) and a reduced ΔE_{ST} of 0.06 eV in 3 wt.% mCBP film, enabling efficient reverse intersystem crossing (k_{RISC} = 1.6×10^5 s^{-1}) without undesirable spectral shifts. This favorable balance translates into OLEDs with a high EQE of 22.2%, narrow electroluminescence (24 nm FWHM), and improved exciton utilization, outperforming the parent **BCz-BN** device under identical fabrication conditions. DFT and vibronic analyses further reveal that the **DBX** unit subtly extends the LUMO and introduces additional low-frequency vibrational modes, providing a mechanistic basis for the reduced ΔE_{ST} and enhanced vibronic coupling. Overall, this work establishes rigid-core engineering as a practical and synthetically accessible strategy for developing high-purity sky-blue MR-TADF emitters for next-generation high-definition and AR/VR display technologies.

Acknowledgements

T.V. thanks SERB for the National Postdoctoral Fellow (File no. PDF/2023/001648). S.M. thanks ANRF for the National Postdoctoral Fellow (File no. PDF/2025/001073). N.S.H. thanks the University Grants Commission (UGC) for the doctoral fellowship (NTA Ref. No. 221610040294). U.D. and S.P. thank the Indian Institute of Science (IISc) for the doctoral fellowship. P.R. thanks IISc and the INDIA-TAIWAN Programme of Cooperation in Science and Technology (Grant No. 2024/IN-TW/07), the Ministry of Human Resource Development (MHRD), India (Grant No: MoE-STARS/STARS-2/2023-0651), and the Indian Council of Medical Research (ICMR) (Grant no: IRPSG-2024-01-02893) for financial support. The authors are grateful to the INF IISc Bangalore for the NMR facility.

Conflicts of Interest

The authors declare no conflicts of interest.

Data Availability Statement

The data that support the findings of this study are available from the corresponding author upon reasonable request.

References

1. Y. Kondo, K. Yoshiura, S. Kitera, et al., "Narrowband Deep-Blue Organic Light-Emitting Diode Featuring an Organoboron-Based Emitter," *Nature Photonics* 13 (2019): 678–682, https://doi.org/10.1038/s41566-019-0476-5.

2. M. Mamada, M. Hayakawa, J. Ochi, and T. Hatakeyama, "Organoboron-Based Multiple-Resonance Emitters: Synthesis, Structure–Property Correlations, And Prospects," *Chemical Society Reviews* 53 (2024): 1624–1692, https://doi.org/10.1039/D3CS00837A.

3. J. M. D. Santos, D. Hall, B. Basumatary, et al., "The Golden Age of Thermally Activated Delayed Fluorescence Materials: Design and Exploitation," *Chemical Reviews* 124 (2024): 13736–14110, https://doi.org/10.1021/acs.chemrev.3c00755.

4. P. Rajamalli, N. Senthilkumar, P.-Y. Huang, C.-C. Wu, H.-W. Lin, and C.-H. Cheng, "New Molecular Design Concurrently Providing Superior Pure Blue, Thermally Activated Delayed Fluorescence and Optical Out-Coupling Efficiencies," *Journal of the American Chemical Society* 139 (2017): 10948–10951, https://doi.org/10.1021/jacs.7b03848.

5. D. Chen, P. Rajamalli, F. Tenopala-Carmona, et al., "Bipyridine-Containing Host Materials for High Performance Yellow Thermally Activated Delayed Fluorescence-Based Organic Light Emitting Diodes With Very Low Efficiency Roll-Off," *Advanced Optical Materials* 8 (2020): 1901283, https://doi.org/10.1002/adom.201901283.

6. G. P. Nanda, B. Sk, N. Yadav, et al., "Ultrathin Non-Doped Thermally Activated Delayed Fluorescence Emitting Layer for Highly Efficient OLEDs," *Chemical Communications* 57 (2021): 13728–13731, https://doi.org/10.1039/D1CC04972K.

7. S. Maity, A. M. T. Muthig, I. Sen, et al., "A [2.2]Isoindolinophanyl-Based Carbene (iPC) Ligand: Synthesis, Electronic and Photophysical Properties, and Application in Photocatalysis**," *Angewandte Chemie International Edition* 63 (2024): 202409115, https://doi.org/10.1002/anie.202409115.

8. C. F. R. Mackenzie, L. Zhang, D. B. Cordes, A. M. Z. Slawin, I. D. W. Samuel, and E. Zysman-Colman, "Bulky Iridium NHC Complexes for Bright, Efficient Deep-Blue OLEDs," *Advanced Optical Materials* 11 (2023): 2201495, https://doi.org/10.1002/adom.202201495.

9. J.-G. Yang, N. Li, J. Li, et al., "A Thermally Activated Delayed Fluorescent Platinum (ii) Complex for Red Organic Light Emitting Diodes with High Efficiencies and Small Roll-Off," *Journal of Materials Chemistry A* 12 (2024): 18977–18985, https://doi.org/10.1039/D4TA02301C.

10. T. Hatakeyama, K. Shiren, K. Nakajima, et al., "Ultrapure Blue Thermally Activated Delayed Fluorescence Molecules: Efficient HOMO–LUMO Separation by the Multiple Resonance Effect," *Advanced Materials* 28 (2016): 2777–2781, https://doi.org/10.1002/adma.201505491.

11. S. Hirata, Y. Sakai, K. Masui, et al., "Highly Efficient Blue Electroluminescence Based on Thermally Activated Delayed Fluorescence," *Nature Materials* 14 (2025): 330–336, https://doi.org/10.1038/nmat4154.

12. K. R. Naveen, H. I. Yang, and J. H. Kwon, "Double Boron-Embedded Multiresonant Thermally Activated Delayed Fluorescent Materials for Organic Light-Emitting Diodes," *Communications Chemistry* 5 (2022): 149, https://doi.org/10.1038/s42004-022-00766-5.

13. R. Keruckiene, A. A. Vaitusionak, M. I. Hulnik, et al., "Is a Small Singlet–Triplet Energy Gap a Guarantee of TADF Performance in MR-TADF Compounds? Impact of the Triplet Manifold Energy Splitting," *Journal of Materials Chemistry C* 12 (2024): 3450–3464, https://doi.org/10.1039/D3TC04397E.

14. E. Tankelevičiūtė, I. D. W. Samuel, and E. Zysman-Colman, "The Blue Problem: OLED Stability and Degradation Mechanisms," *Journal of Physical Chemistry Letters* 15 (2024): 1034–1047.

15. H.-X. Ni, L. Yuan, and Y.-X. Zheng, "Spectral Narrowing Strategies in Multiple Resonance Thermally Activated Delayed Fluorescence Materials," *Chemphyschem* 26 (2025): 202500201.

16. Q. Wu, J. Li, D. Liu, et al., "Dual Emission from Donor-Modified MR-TADF Emitter: Evidence for Coexistence of TICT and MR Excited States," *Dyes and Pigments* 217 (2023): 111421, https://doi.org/10.1016/j.dyepig.2023.111421.

17. X. Song, S. Shen, S. Zou, et al., "Efficient Narrowband Organic Light-Emitting Devices Based on Multi-Resonance TADF Emitters with Secondary Donor," *Chemical Engineering Journal* 467 (2023): 143557, https://doi.org/10.1016/j.cej.2023.143557.

18. X.-L. Liu, W.-L. Wu, R.-J. Wang, et al., "Blue-Hazard-Free Single-Emissive-Layer White Organic LEDs Based on an Anti-Quenching Narrowband Blue Emitter," *FlexMat* 1 (2025): 70024.

19. Y. Zhang, D. Zhang, J. Wei, Z. Liu, Y. Lu, and L. Duan, "Multi-Resonance Induced Thermally Activated Delayed Fluorophores for Narrowband Green OLEDs," *Angewandte Chemie International Edition* 58 (2019): 1911266, https://doi.org/10.1002/anie.201911266.

20. S. Oda, W. Kumano, T. Hama, R. Kawasumi, K. Yoshiura, and T. Hatakeyama, "Carbazole-Based DABNA Analogues as Highly Efficient Thermally Activated Delayed Fluorescence Materials for Narrowband Organic Light-Emitting Diodes," *Angewandte Chemie International Edition* 60 (2021): 2882–2886, https://doi.org/10.1002/anie.202012891.

21. X. Xiao, B. Lei, D. Wu, and Z. Bin, "Medium-Ring″ Strategy Enables High-Performance Narrowband Pure-Blue Multi-Resonance Emitters: Boost Provided by a Unique Perpendicular Geometry," *Chemical Communications* 59 (2023): 6556–6559.

22. C. Lee, Y.-T. Lee, C.-Y. Chan, et al., "Regioisomer Effect of Pyrene on Multi-Resonance Emitters and Their Application for Hyperfluorescence Organic Light-Emitting Diodes," *Advanced Optical Materials* 13 (2025): 2402862, https://doi.org/10.1002/adom.202402862.

23. G. Chen, S.-W. Chen, Y. Su, et al., "Highly Efficient Organic Light-Emitting Diodes Based on Spatially Compacted π-Stacked MR-TADF Emitters," *Advanced Functional Materials* 35 (2025): 2501039, https://doi.org/10.1002/adfm.202501039.

24. F. Zheng, X.-L. Liu, L. Xing, et al., "Highly Efficient Circularly Polarized Luminescence Based on Center-Chiral Frustrated Lewis Pairs," *Angewandte Chemie International Edition* 64 (2025): 202504057, https://doi.org/10.1002/anie.202504057.

25. D. Barman, Y. Tsuchiya, and C. Adachi, "Horizontally Oriented MRCT-Type TADF Emitter Achieving EQE Over 40% for Sky-Blue OLED," *Nature Communications* 16 (2025): 5023, https://doi.org/10.1038/s41467-025-59893-x.

26. Z. Xue, Z. Xiao, Y. Zou, et al., "A Mesityl-Functionalized Double-Boron–Nitrogen–Oxygen-Embedded Multi-Resonance Framework Achieves Anti-Quenching Narrowband Deep-Blue Electroluminescence with EQE Over 30% and CIE y of 0.046," *Chemical Science* 16 (2025): 3655–3661, https://doi.org/10.1039/D4SC07503J.

27. T. Viswanathan, N. Yadav, N. S. H. Nandish, S. Pal, A. K. Mazumdar, and P. Rajamalli, "Rational Rigid-Core Design Realises Efficient and Colour-Pure Sky-Blue MR-TADF Emission in Boron-Nitrogen Functionalised Dibenzo-Xanthene," *Chemistry - An Asian Journal* 20 (2025): 202401439.

28. J. Wang, Y. Yasuda, Y. Ren, et al., "A Multi-Resonant Thermally Activated Delayed Fluorescence Emitter with a Twisted Second-Generation Carbazole Dendron Showing Suppressed Concentration Quenching and its Use in Solution-Processed Organic Light-Emitting Diodes," *Organic Chemistry Frontiers* 12 (2025): 3279–3287, https://doi.org/10.1039/D5QO00146C.

29. Y. Gao, S. Wu, G. Shan, and G. Cheng, "Recent Progress in Blue Thermally Activated Delayed Fluorescence Emitters and Their Applications in OLEDs: Beyond Pure Organic Molecules With Twist D-π-A Structures," *Micromachines* 13 (2022): 2150, https://doi.org/10.3390/mi13122150.

30. F. Neese, "The ORCA Program System," *WIREs Computational Molecular Science* 2 (2012): 73–78.

31. R. K. Sanyam and A. Mondal, "Cost-Effective Approach for Modeling of Multiresonant Thermally Activated Delayed Fluorescence Emitters," *Journal of Chemical Theory and Computation* 19 (2023): 9290–9301, https://doi.org/10.1021/acs.jctc.3c01147.

32. K. Tvingstedt, J. Benduhn, and K. Vandewal, "temperature Dependence of the Spectral Line-Width of Charge-Transfer State Emission in Organic Solar Cells; Static vs. Dynamic Disorder," *Materials Horizons* 7 (2020): 1888–1900.

33. K. Shizu and H. Kaji, "Comprehensive Understanding of Multiple Resonance Thermally Activated Delayed Fluorescence Through Quantum Chemistry Calculations," *Communications Chemistry* 5 (2022): 53, https://doi.org/10.1038/s42004-022-00668-6.

34. T. Viswanathan, Y. Kusakabe, U. Acharyya, H. Kaji, and P. Rajamalli, "Benzoylfuran- and Thiophene-Based Thermally Activated Delayed Fluorescence Emitters for Organic Light-Emitting Diodes," *ACS Applied Optical Materials* 2 (2024): 2409–2415.

35. G. P. Nanda, R. Suraksha, B. Sk, T. Viswanathan, and P. Rajamalli, "Improving the External Quantum Efficiency and Minimizing the Efficiency Roll-Off in OLEDs: A Study on the Optimization of Donor Linkage and Acceptor Nitrogen Atom Positions in TADF emitters," *Journal of Materials Chemistry C* 13 (2025): 14953–14961, https://doi.org/10.1039/D5TC01563D.

Supporting Information

Additional supporting information can be found online in the Supporting Information section.

Supporting File: smll73625-sup-0001-SuppMat.pdf.